Direct Imaging of Integer and Half-Integer Josephson Vortices in High-T_c Grain Boundaries

J. R. Kirtley, C. C. Tsuei, Martin Rupp, J. Z. Sun, Lock See Yu-Jahnes, A. Gupta, and M. B. Ketchen
IBM Thomas J. Watson Research Center, P.O. Box 218, Yorktown Heights, New York 10598

K. A. Moler
Department of Physics, Princeton University, Princeton, New Jersey 08544

M. Bhushan
Department of Physics, State University of New York at Stony Brook, Stony Brook, New York 11794
(Received 18 August 1995)

We have used a high-resolution scanning SQUID microscope to directly image conventional ($h/2e$) Josephson vortices trapped in grain boundaries, and half-integer ($h/4e$) Josephson vortices trapped at the tricrystal point, of the high-T_c superconductor $YBa_2Cu_3O_{7-\delta}$ grown on tricrystal substrates of $SrTiO_3$. Our observation of the half-integer vortex at the tricrystal point is the first direct demonstration of the positive paramagnetic Meissner effect in a polycrystalline high-T_c film. In addition, our images provide the first direct measurement of the Josephson penetration depth.

PACS numbers: 74.60.Ge

Half-integer flux quantization is a powerful tool for probing the symmetry of the superconducting gap in both $YBa_2Cu_3O_{7-\delta}$ and other unconventional superconductors. It was first predicted by Bulaevski, Kuzii, and Sobyanin [1], and first related to unconventional superconductivity by Geshkenbein and Larkin [2]. Geshkenbein, Larkin, and Barone predicted that half-integer flux quanta would be spontaneously generated at the intersection of three grain boundaries if there is an odd number of sign changes of the normal component of the superconducting order parameter in a closed loop around the tricrystal point [3]. Braunisch *et al.* [4] and Sigrist and Rice [5] used this spontaneous magnetization mechanism to explain the positive paramagnetic Meissner screening often observed in polycrystalline films of high-T_c superconductors. A number of demonstrations of this effect in specialized geometries have been made, including interference measurements in single crystal $YBa_2Cu_3O_{7-\delta}$-Pb SQUIDS [6,7] and tunnel junctions [8], direct imaging of half-integer flux quanta in a tricrystal ring geometry [9], and in a thin film $YBa_2Cu_3O_{7-\delta}$-Pb geometry [10]. Evidence for this effect in current-voltage measurements of a grain boundary junction at the tricrystal point in a geometry very similar to that used by Tsuei [9] was reported by Miller *et al.* [11].

We report here the first direct experimental observation of spontaneous magnetization in a controlled geometry tricrystal point in a thin film of $YBa_2Cu_3O_{7-\delta}$. This technique has several advantages. First, the observation of half-flux quanta in a geometry that requires no photolithographic patterning makes sample fabrication significantly easier. Second, the fields associated with the half-flux quantum in the form of a Josephson vortex are about 50 times larger than those in a 50 μm diameter ring, making measurements using less sensitive techniques than scanning SQUID microscopy feasible. Third, these experiments provide a direct measurement of the Josephson penetration depth λ_J. Recently Fischer *et al.* have imaged $YBa_2Cu_3O_{7-\delta}$ Josephson grain boundary junctions in the short junction limit $\lambda_J \sim w$, where w is the width of the junction, using a low-temperature scanning electron microscope [12]. In this limit the spatial variation of the imaged supercurrent is not directly related to the Josephson penetration depth.

Our samples [9] consisted of thin films of the high-temperature superconductor $YBa_2Cu_3O_{7-\delta}$ 120 nm thick grown epitaxially on *c*-axis up tricrystal substrates of $SrTiO_3$. The tricrystal substrates were fabricated from (100) component crystals that were reoriented, polished, and fused together to form three approximately 30° bicrystals that meet at a single point (Fig. 1). The grain boundaries of $YBa_2Cu_3O_{7-\delta}$ epitaxially grown on the bicrystal substrates have been well characterized by electron microscopy, by their resistive transitions, and by their current-voltage characteristics [13–16].

The samples were imaged using a high-resolution scanning SQUID microscope (SSM) [17–19]. In our microscope [20] a pickup loop integrated into a low-T_c superconducting quantum interference device (SQUID) sensor is mechanically scanned about a micron above the sample surface. The signal is proportional to the normal component of the magnetic field at the surface. Our pickup loop, with the smallest diameter (4 μm center-to-center loop diameter, with 0.8 μm linewidth) and most carefully shielded pickup loop fabricated to date, allows us to spatially resolve the Josephson penetration length. All the images in this paper were taken with the sample at 4.2 K.

The present tricrystal geometry produces an odd number of negative Josephson critical currents around a path enclosing the tricrystal point, if the order parameter of $YBa_2Cu_3O_{7-\delta}$ has *d*-wave symmetry [5,9]. In the absence of a supercurrent, any choice of the superconducting phase for the three subsections of the $YBa_2Cu_3O_{7-\delta}$ film

 0031-9007/96/76(8)/1336(4)$06.00

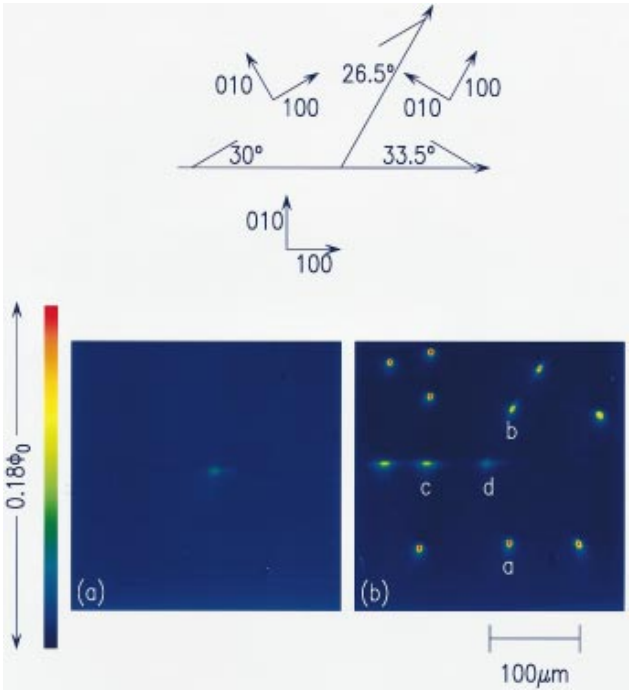

FIG. 1 (color). Schematic diagram for the tricrystal (100) $SrTiO_3$ substrate, with two scanning SQUID microscope images of a blanket coverage of $YBa_2Cu_3O_{7-\delta}$ on the substrate. When cooled in nominally zero field (a) the only flux trapped in the sample is a half-flux quantum at the tricrystal point. When the sample is cooled in a field of 3×10^{-7} T, a half-flux quantum is trapped at the tricrystal point, four Josephson vortices are trapped along the grain boundaries, and seven bulk vortices are visible, trapped apart from the grain boundaries. The full scale variation in flux through the SQUID sensor in these images is $0.18\Phi_0$.

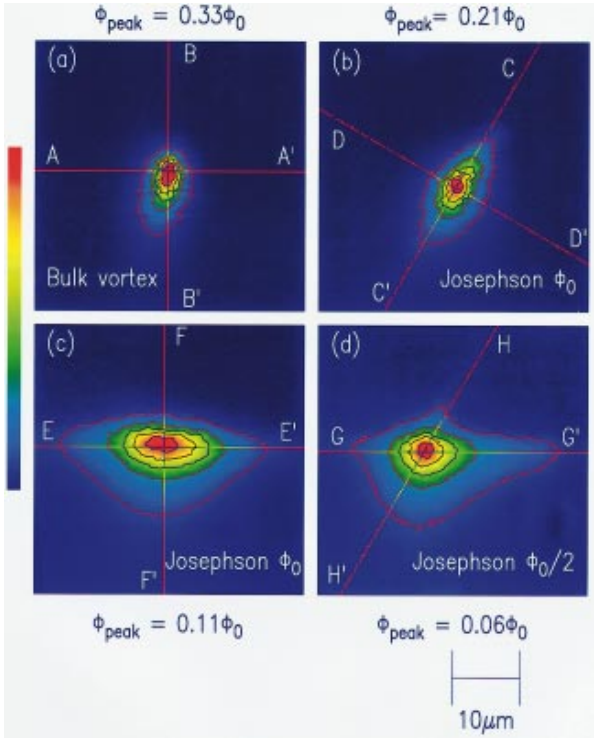

FIG. 2 (color). Expanded images of some of the vortices labeled in Fig. 1: (a) A bulk vortex, (b) a Josephson vortex trapped on the diagonal grain boundary, (c) a Josephson vortex trapped on the horizontal grain boundary, and (d) a half quantum Josephson vortex trapped at the tricrystal point.

will involve a highly energetically unfavorable Josephson coupling energy $E_j = I_c \cos(\phi_i - \phi_j)$ across at least one of the grain boundaries [1,2]. This energy is reduced by the generation of a spontaneous supercurrent around the tricrystal point. In the limit $2\pi L I_c/\Phi_0 \gg 1$, where L is the effective inductance of the tricrystal point and $\Phi_0 = h/2e$ is the superconducting flux quantum, this supercurrent will generate exactly half of a flux quantum $(h/4e)$ at the tricrystal point [5]. Josephson $(h/2e)$ vortices also can be trapped along the grain boundaries, and bulk $(h/2e)$ vortices can be trapped in the film away from the grain boundaries.

Figure 1(a) shows an SSM image of the central region of the sample, cooled in nominally zero field. The visible flux is a $h/4e$ Josephson vortex at the tricrystal point. Figure 1(b) shows an image of the same area recooled through T_c in a field of 3×10^{-7} T. In this image there is a half-flux quantum at the tricrystal point, two Josephson vortices along each of the horizontal and diagonal grain boundaries, and seven bulk flux quanta away from the grain boundaries.

Figure 2 shows expanded images of the vortices labeled (a)–(d) in Fig. 1(b). Contour lines have been placed on the data at 0.1, 0.3, 0.5, 0.7, and 0.9 of the full scale amplitudes. The solid lines in Fig. 3 are cross sections through the data of Fig. 2, as indicated by the contrasting lines. The dotted lines in Fig. 3 are modeling of the experimental cross sections as follows.

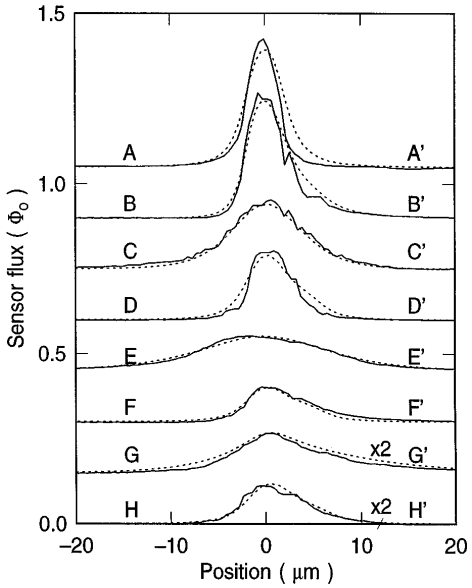

FIG. 3. The solid lines are cross sections through the data as indicated by the contrasting lines in Fig. 2. The dashed lines are fits to the data as described in the text.

The field at a distance r from a superconducting bulk vortex [Fig. 2(a)] in the limit $r \gg \lambda_L, t$, where λ_L is the London penetration depth and t is the film thickness, is given by [21–23]

$$\vec{B}(\vec{r}) = (\Phi_0/2\pi)\vec{r}/|r|^3 . \quad (1)$$

The effective pickup area of a circular ring is closely approximated by the geometric mean area $\pi r_{\rm in} r_{\rm out}$ [24]. We therefore use an octagonal ring of diameter 3.9 μm for our modeling. There is an additional pickup area from redirection of flux by the ground planes shielding the leads. We model this as an area 4 μm squared adjacent to the octagonal loop, with $\frac{1}{3}$ of the flux passing through this area entering the SQUID loop. This additional area produces slight "tails" in the images directly below the vortices. The dashed lines labeled AA' and BB' in Fig. 3 are fits to the data, using the fields of Eq. (2), numerical integrating over the pickup loop area, with 10° between the plane of the loop and the surface, and using the height of the loop as a fitting parameter. The effective height is 1.8 μm. The height estimated from the sensor geometry is 0.7 μm. The height determined from fitting the bulk vortices fixes the effective height for modeling the Josephson vortices.

We model the grain boundary as two slabs of superconductors spaced by d centered about $y = 0$ in the x-z plane. Inside a Josephson junction, the phase ϕ is described by the sine-Gordon equation [25,26]

$$\vec{\nabla}^2\phi = \sin\phi/\lambda_J^2 . \quad (2)$$

The phase ϕ is related to the current flowing perpendicular to the junction, $\vec{J} = J(x, y = 0)\hat{y}$, by the Josephson relation $J(x, y = 0) = J_c \sin[\phi(x)]$. A solution to Eq. (3) which is centered about $x = 0$ and which goes to zero as $|x| \to \infty$ is

$$\phi(x) = 4\tan^{-1}(ae^{-|x|/\lambda_J}) . \quad (3)$$

The flux/unit length passing through the junction is

$$\frac{d\Phi}{dx} = \frac{\Phi_0}{2\pi}\frac{(-4a)}{\lambda_J}\frac{e^{-|x|/\lambda_J}}{1 + a^2e^{-2|x|/\lambda_J}} . \quad (4)$$

If the grain boundary has two sections, positive x and negative x, the flux in each section is given by $(\Phi_0/2\pi)4\tan^{-1} a$. A $(h/2e)$ Josephson vortex has $a = 1$, and

$$B_z(x, y = 0) = B_0 \,\mathrm{sech}(x/\lambda_J) , \quad (5)$$

with $B_0 = \Phi_0/\pi d\lambda_J$ [26]. Inside a superconductor, the London theory gives $\vec{\nabla}^2\vec{B} = \vec{B}/\lambda_L^2$. Using London theory to describe the field inside the superconductor is strictly valid only if no current flows through the sample boundary. It is a reasonable approximation for $\lambda_L \ll \lambda_J$. Neglecting the x derivative in the Laplacian is an approximation of order $(\lambda_L/\lambda_J)^2$, and leads to

$$B(x, y) = B_0 \,\mathrm{sech}(x/\lambda_J)e^{-|y|/\lambda_L}, \quad (6)$$

with $d = 2\lambda_L$.

Once the fields at the surface are known, the fields at height z are derived by

$$b_z(k_x, k_y, z) = \exp(-\sqrt{k_x^2 + k_y^2}\, z)b_z(k_x, k_y, 0) , \quad (7)$$

where b_z is the two-dimensional Fourier transform of the field $B_z(\vec{r})$, and k_x and k_y are the wave vectors in the x and y directions, respectively [27]. The SSM signals are then calculated by numerically integrating over the effective pickup loop area, using the same parameters as for the bulk vortex outlined above. The cross sections in Fig. 3 labeled CC'–FF' are fits of Eq. (7) to the data, with $\lambda_L = 150$ nm, and using the Josephson penetration depth λ_J as the only fitting parameter. We find $\lambda_J = 5.0$ μm for the Josephson vortices along the horizontal grain boundary, while $\lambda_J = 2.2$ μm along the diagonal grain boundary. These lengths were uniform along the grain boundaries in this sample, and were reproducible in two other samples with the same tricrystal substrate geometry. The uncertainties in the penetration depths are dominated by uncertainties in the fits, which we estimate to be $1.7 < \lambda_J < 2.7$ μm for the diagonal grain boundary, and $4.5 < \lambda_J < 5.6$ μm for the horizontal grain boundary, using a criterion of a doubling of the variance from the least squares fit value.

For the half-flux quantum at the tricrystal point, we generalize Eq. (5) so that a and λ_J are different for three grain boundaries away from the tricrystal point. The condition that the magnetic field at the tricrystal point varies smoothly implies that the factor $a_i/\lambda_{Ji}(1 + a_i^2)$ is the same for each grain boundary. Combining this with the condition that the total flux at the tricrystal point $\Phi = \sum_i(\Phi_0/2\pi)4\tan^{-1}(a_i) = \Phi_0/2$ uniquely determines the a_i's for a given set of λ_J's. The dashed lines GG' and HH' in Fig. 3 are fits of this model, using a decay of the fields perpendicular to the grain boundaries set by the London penetration depth $\lambda_L = 150$ nm, with the effective height set by fits to the bulk vortex, using the three Josephson penetration depths as fitting parameters. The best fit, holding the total flux at $h/4e$ (Fig. 3, curves GG' and HH'), occurs for $\lambda_1 = 4.2$ μm for the horizontal grain boundary to the left of the tricrystal point, $\lambda_2 = 8.2$ μm to the right of the tricrystal point, and $\lambda_3 = 2.0$ μm for the diagonal grain boundary.

Measurements of the critical currents of microbridges 10 μm wide fabricated on the same samples that we imaged had critical current densities J_c that varied from 1.5×10^5 to 4×10^3 A/cm^2, widely varying resistive transitions and current-voltage characteristics, and nonideal Frauenhofer patterns. In contrast, the images of the Josephson vortices are remarkably homogeneous. The range of measured critical currents corresponds to a range

of expected Josephson penetration depths [25], $\lambda_J^2 = \Phi_0/2\pi d\mu_0 J_c$, of $4.7 > \lambda_j > 0.76$ μm. Numerical simulations [28] indicate that the Josephson penetration depth for our actual geometry, two 120 nm thick films butted together, can be as much as a factor of 2 larger than for the two semi-infinite planes for which the standard formula is derived. Therefore our measured Josephson penetration depths are within the range expected from transport measurements. The measured critical currents may be more inhomogeneous than the images because the bridges were made several mm from the tricrystal point, whereas the scanning SQUID microscope images were of areas 400 μm wide centered at the tricrystal point. Further, the processing required to define microbridges for the critical current measurements could change the characteristics of the sample. Direct imaging of the Josephson vortices is a less invasive technique to characterize grain boundaries.

The model of the tricrystal vortex as having $h/4e$ total flux predicts a slightly ($\sim$15%) larger SQUID microscope signal than is observed. This reduction in apparent flux below $\Phi_0/2$ could be an indication of time reversal symmetry breaking at the tricrystal point [29]. However, our modeling could be inaccurate because the magnetic fields inside the grain boundary are modeled assuming an infinitely thick film, while the fields above the surface are modeled assuming a two-dimensional current distribution in the sample plane, and the fields parallel and perpendicular to the grain boundaries are treated independently, even at the tricrystal point. Further, flux quantization below $\Phi_0/2$ can be expected if the figure of merit $2\pi LI_c$ is of the same size as Φ_0, where L is an effective inductance of the tricrystal point and I_c is its effective critical current. It is difficult to know whether this is an important factor, since combining our measured variation in Josephson penetration depths, measured critical current densities, and an estimate of our grain boundary inductance of $\sim$0.8 pH/μm gives a variation for $2\pi LI_c/\Phi_0$ from 0.2 to 70. Qualitatively similar results were obtained for $h/2e$ and $h/4e$ Josephson vortices trapped in 50 μm diameter, 120 nm thick, thin film disks of $YBa_2Cu_3O_{7-\delta}$ covering the tricrystal point and the horizontal and diagonal grain boundaries, but modeling of these vortices may be complicated by the finite disk size.

In conclusion, imaging of Josephson vortices in a tricrystal sample of $YBa_2Cu_3O_{7-\delta}$ provides an elegant and useful means of detecting the half-integer flux quantum effect, as well as a method for directly measuring the Josephson penetration depth in high-T_c grain boundaries.

The scanning SQUID microscope used here was partially supported by the Consortium for Superconducting Electronics, with funding from Advanced Research Projects Agency Contract No. MDA972-90-C-0021. The technical assistance of G. Trafas is greatly appreciated.

[1] L. N. Bulaevski, V. V. Kuzii, and A. A. Sobyanin, JETP Lett. **25**, 290 (1977).
[2] V. B. Geschkenbein and A. I. Larkin, Phys. Rev. B **36**, 235 (1987).
[3] V. B. Geschkenbein, A. I. Larkin, and A. Barone, Phys. Rev. B **36**, 235 (1987).
[4] W. Braunisch *et al.*, Phys. Rev. Lett. **68**, 1908 (1992).
[5] Manfred Sigrist and T. M. Rice, J. Phys. Soc. Jpn. **61**, 4283 (1992).
[6] D. A. Wollman *et al.*, Phys. Rev. Lett. **71**, 2134 (1993).
[7] D. A. Brawner and H. R. Ott, Phys. Rev. B **50**, 6530 (1994).
[8] D. A. Wollman *et al.*, Phys. Rev. Lett. **74**, 797 (1995).
[9] C. C. Tsuei *et al.*, Phys. Rev. Lett. **73**, 593 (1994).
[10] A. Mathai *et al.*, Phys. Rev. Lett. **74**, 4523 (1995).
[11] J. H. Miller *et al.*, Phys. Rev. Lett. **74**, 2347 (1995).
[12] G. M. Fischer *et al.*, Science **263**, 1112 (1994).
[13] S. E. Babcock and D. C. Larbelestier, J. Phys. Chem. Solids **55**, 1125 (1995).
[14] R. Gross, in *Interfaces in High-T_c Superconducting Systems*, edited by S. L. Shinde and D. A. Rudman (Springer-Verlag, New York, 1994), pp. 176–209.
[15] D. Dimos, P. Chaudhari, and J. Mannhart, Phys. Rev. B **41**, 4038 (1990).
[16] M. S. Chisholm and S. J. Pennycook, Nature (London) **351**, 47 (1991).
[17] F. P. Rogers, BS/MS thesis, MIT, 1983.
[18] L. N. Vu, M. S. Wistrom, and D. J. van Harlingen, Appl. Phys. Lett. **63**, 1693 (1993).
[19] R. C. Black *et al.*, Appl. Phys. Lett. **62**, 2128 (1993).
[20] J. R. Kirtley *et al.*, Appl. Phys. Lett. **66**, 1138 (1995).
[21] Judea Pearl, J. Appl. Phys. **37**, 4139 (1966).
[22] V. G. Kogan, A. Yu. Simonov, and M. Ledvij, Phys. Rev. B **48**, 392 (1993).
[23] A. M. Chang *et al.*, Europhys. Lett. **20**, 645 (1992).
[24] J. R. Kirtley *et al.*, Nature (London) **373**, 225 (1995).
[25] C. S. Owen and D. J. Scalapino, Phys. Rev. **164**, 538 (1967).
[26] John R. Clem and Mark W. Coffey, Phys. Rev. B **42**, 6209 (1990).
[27] Bradley J. Roth, Nestor G. Sepulveda, and John P. Wikswo, Jr., J. Appl. Phys. **65**, 361 (1988).
[28] W. H. Chang, IEEE Trans. Magn. **17**, 764 (1981).
[29] M. Sigrist, D. B. Bailey, and R. B. Laughlin, Phys. Rev. Lett. **74**, 3249 (1995).